Theory and Normal-Mode Analysis of Change in Protein Vibrational Dynamics on Ligand Binding

Kei Moritsugu,*,†,‡ Brigitte M. Njunda,§ and Jeremy C. Smith†

Center for Molecular Biophysics, University of Tennessee/Oak Ridge National Laboratory, 1 Bethel Valley Road, Oak Ridge, Tennessee 37831, Research Program for Computational Science, RIKEN, 2-1 Hirosawa, Wako, Saitama 351-0198, Japan, and Computational Molecular Biophysics, Interdisciplinary Center for Scientific Computing (IWR), University of Heidelberg, Im Neuenheimer Feld 368, Heidelberg 69120, Germany

Received: October 9, 2009

The change of protein vibrations on ligand binding is of functional and thermodynamic importance. Here, this process is characterized using a simple analytical "ball-and-spring" model and all-atom normal-mode analysis (NMA) of the binding of the cancer drug, methotrexate (MTX) to its target, dihydrofolate reductase (DHFR). The analytical model predicts that the coupling between protein vibrations and ligand external motion generates entropy-rich, low-frequency vibrations in the complex. This is consistent with the atomistic NMA which reveals vibrational softening in forming the DHFR−MTX complex, a result also in qualitative agreement with neutron-scattering experiments. Energy minimization of the atomistic bound-state (B) structure while gradually decreasing the ligand interaction to zero allows the generation of a hypothetical "intermediate" (I) state, without the ligand force field but with a structure similar to that of B. In going from I to B, it is found that the vibrational entropies of both the protein and MTX decrease while the complex structure becomes enthalpically stabilized. However, the relatively weak DHFR:MTX interaction energy results in the net entropy gain arising from coupling between the protein and MTX external motion being larger than the loss of vibrational entropy on complex formation. This, together with the I structure being more flexible than the unbound structure, results in the observed vibrational softening on ligand binding.

1. Introduction

The binding of ligands to proteins is a crucial element of cellular function.[1−5] Ligand binding perturbs the protein potential energy surface and thus the associated protein dynamics, and may be accompanied by conformational change.[6−8] Methods have been investigated for predicting ligand-binding sites[9] and ligand-bound protein structures from unbound structures and the associated fluctuations,[9−15] and computational searches have been performed for pathways between bound and unbound states.[16] Ligand binding may initiate perturbations propagating to remote sites of the proteins, leading dynamically to functional motions.[17−21] The change in protein equilibrium fluctuations on ligand binding has been examined in several computational studies[22−31] and experimentally using inelastic neutron-scattering experiments,[32] NMR,[33,34] X-ray crystallography,[34] and fluorescence spectroscopy.[35,36]

The present study derives an analytical model of ligand-binding dynamics and applies it to interpret atomistic simulation of dihydrofolate reductase (DHFR) with and without a bound ligand molecule, the cancer drug methotrexate (MTX). DHFR catalyzes the reduction of dihydrofolate to tetrahydrofolate in the presence of the nicotinamide adenine dinucleotide phosphatate cofactor,[37−41] and MTX is a folate antagonist of DHFR.[42] A change of the vibrational density of states, $g(\omega)$, on binding MTX to DHFR at 120 K has been observed using inelastic neutron scattering:[32] $g(\omega)$ increases in the lowest frequency range, $\omega < \sim 20$ cm^{-1}; i.e., the complexed protein is more vibrationally flexible than the uncomplexed form, leading to an increase of entropy on binding.

We aim here at deriving a simplified physical picture of how dynamical softening on ligand binding occurs. Previous calculations, on the binding of a water molecule to bovine pancreatic trypsin inhibitor (BPTI), revealed the contribution of water external (rigid-body) motion to the increased flexibility of the complex.[28,29] To further examine this, we construct a simplified analytical model comprising a ligand coupling to a protein vibration via a harmonic spring. Frequency shifts of the vibrations are analyzed, allowing the origin of the vibrational entropy gain on ligand binding to be understood.

The model system derivation is then applied to analyze the atomistic DHFR + MTX system. To do this, the binding process is considered to generate coupling between the protein vibrations and the internal and external motions of the ligand. Normal-mode analysis (NMA), making the harmonic approximation to the potential energy, which has been applied to characterize both collective, low-frequency motions[43] and local, high-frequency vibrations[44,45] in protein, is used to derive the vibrational modes. However, a complication arises because the structures of the bound and unbound protein states are in general different owing to the rotational motions of two domains, the adenosine binding domain and the loop domain,[46] and so the vibrational modes of the two states will also be different. Consequently, here, ligand binding is separated into two processes: the conformational change on binding and the generation of ligand interaction. We focus here on the latter process, i.e., how the interaction with the ligand perturbs the dynamics of the complex.

To perform the above separation, a hypothetical intermediate state with the bound-state structure but without the ligand

* To whom correspondence should be addressed. Tel.: +81-48-462-1628. Fax: +81-48-462-1625. E-mail: moritsuguk@riken.jp.
† University of Tennessee/Oak Ridge National Laboratory.
‡ RIKEN.
§ University of Heidelberg.

10.1021/jp909677p
Published on Web 12/31/2009

must be characterized. To do this, iterative energy minimizations of the experimental all-atom bound-state structure are performed while decreasing the protein−ligand interaction step-by-step. This procedure is complete when the protein−ligand interaction is zero, at which point the intermediate state is determined. The vibrational density of states and the vibrational entropy are then calculated and analyzed along the "reaction coordinate" defined by the binding interaction strength, decomposing the results into the contributions of the protein and ligand internal and external motions. This decomposition allows the origin of vibrational thermodynamic change on ligand binding to be understood in the context of the analytical "ball-and-spring" model.

2. Theory and Methods

On ligand binding, protein dynamics is changed by two effects: the change in conformation of the protein from the unbound (U) to the bound (B) state and the interaction between the protein and the ligand. In the present study the ligand binding is decomposed into these two processes, as sketched in Figure 1a. First, the protein changes conformation from U to the intermediate state (I) (process 1) with the protein adopting the structure it has when the ligand is bound, but without the ligand. The second process is the generation of protein−ligand interaction from I to the B state (process 2).

Here, we focus on process 2, i.e., the effect of the ligand force field on the vibrational dynamics with a constant protein structure. To do this, first, the coupling of protein and ligand motion is considered using a simple analytical model, the derivation of which is described in section 2.1. Next, the applicability of the analytical model is evaluated by examining atomistic dynamics of the DHFR (+MTX) system. For simplicity, the harmonic approximation is applied to the DHFR (+MTX) vibrations using NMA, and thus anharmonic contributions to the dynamics are neglected.

2.1. One-Dimensional Model System: Coupling Protein and Ligand Modes. On generation of the protein:ligand interaction during process 2, there occurs coupling between the protein and ligand motions. In addition, the number of internal degrees of freedom increases by 6, i.e., by the number of the protein and ligand external degrees of freedom minus the number of external degrees of freedom of the complex ($6 + 6 - 6 = 6$). The protein external motion can be assumed as fixed in this study because the number of degrees of freedom of DHFR (number of protein atoms: $N_P = 2569$) is much larger than that of MTX (number of ligand atoms: $N_L = 54$). Therefore, the missing six degrees of freedom are considered as ligand external motions coupling to protein vibrations. The coupling of protein vibration and ligand external motion has been shown to lead to softening of vibrations in complexes.[28,29]

Here, we consider two simple analytical model systems, both comprising only one protein and one ligand degree of freedom. In model I the two vibrations are coupled, mimicking the situation that a protein vibration is coupled with a ligand internal vibration, while model E includes a free degree of freedom coupling to a vibration (i.e., one harmonic constraint is relaxed from model I), mimicking the coupling of a protein vibration with a ligand external motion. Therefore, this analytical model study simplifies the overall protein−ligand interaction by decomposing it into the coupling of each protein vibrational mode with each of the ligand internal and external motions.

In model I (Figure 1b1), the protein vibration (corresponding to displacement, x_P, and frequency, ω_p) and the ligand vibration

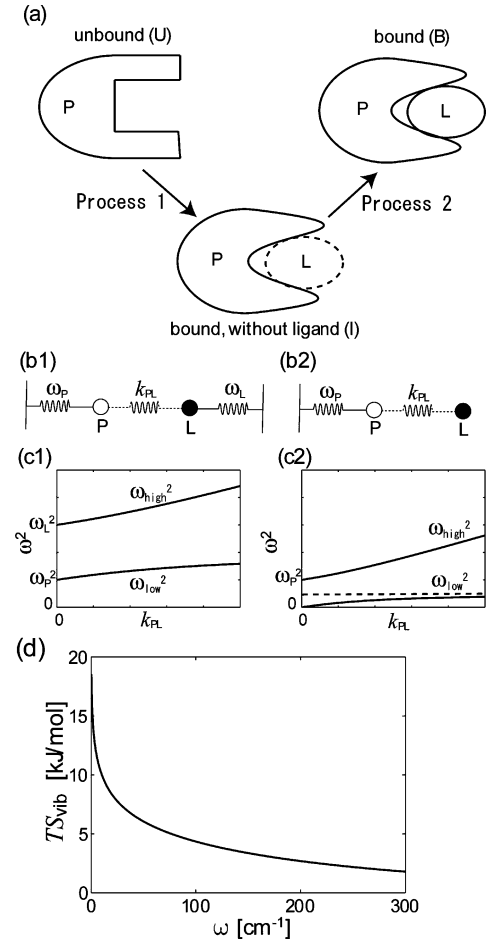

Figure 1. (a) Schematic drawing of ligand (L)-binding process to protein (P). Overall pathway from the unbound (U) to the bound (B) state is decomposed into the process of protein conformational change (process 1) from U to an intermediate state (I) with the bound-state protein structure but without the ligand, and the subsequent process of ligand binding (process 2) from I to B. (b) Analytical models of coupling between protein and ligand degrees of freedom. (b1) Protein vibration coupling to ligand vibrational motion. (b2) Protein vibration coupling to ligand external motion. In (c) the resulting vibrational frequencies (ω_{low} and ω_{high}) are shown as a function of the coupling constant (k_{PL}). Dashed is an asymptotic line at $\omega^2 = \omega_P^2/2$. (d) Vibrational entropy of a harmonic vibration shown as a function of ω.

(x_L, ω_L) are coupled with force constant k_{PL}. The internal energy of the system is given by

$$E = E_0 + E_{int} = \frac{1}{2}\omega_P^2 x_P^2 + \frac{1}{2}\omega_L^2 x_L^2 + \frac{1}{2}k_{PL}(x_P - x_L)^2 \quad (1)$$

Neglecting the masses of both the protein and ligand, or taking the coordinates as mass-weighted (as is the case with the NMA), the resulting two frequencies, calculated by diagonalizing the Hessian matrix from eq 1, are given by

$$\omega^2 = \frac{(\omega_P^2 + \omega_L^2) + 2k_{PL} \pm \sqrt{(\omega_P^2 - \omega_L^2)^2 + 4k_{PL}^2}}{2} \quad (2)$$

Figure 1c1 shows the two frequencies of the complex, ω, schematically as a function of k_{PL}. Both vibrations of the complex shift to higher frequencies upon coupling.

Model E, shown in Figure 1b2, induces an additional vibrational mode corresponding to mixing of the ligand external motion with the protein vibration. The internal energy is then given by

$$E = E_0 + E_{\text{int}} = \frac{1}{2}\omega_P^2 x_P^2 + \frac{1}{2}k_{PL}(x_P - x_L)^2 \qquad (3)$$

and the resulting frequencies are

$$\omega^2 = \frac{\omega_P^2 + 2k_{PL} \pm \sqrt{\omega_P^4 + 4k_{PL}^2}}{2} \qquad (4)$$

Figure 1c2 shows schematically that the coupling in eq 3 generates a low-frequency vibration of the complex, ω_{low}, in the region $\omega_{\text{low}}^2 < \omega_P^2/2$ (where ω_p is the protein frequency without coupling) although the other complex vibration, ω_{high}, is shifted to higher frequency than ω_p; i.e., $\omega_{\text{high}} > \omega_p$.

The vibrational entropy of a harmonic oscillator is given by[47]

$$S_{\text{vib}}(\omega)/k_B = \frac{\hbar\omega/k_BT}{e^{\hbar\omega/k_BT} - 1} - \ln(1 - e^{-\hbar\omega/k_BT}) \qquad (5)$$

where $h = 2\pi\hbar$ is the Planck constant. Figure 1d shows the frequency dependence of $S_{\text{vib}}(\omega)$ (calculated in units of energy, i.e., TS, with $T = 300$ K). The vibrational entropy is dominated by low-frequency vibrations and decreases strongly with ω. Thus, a large vibrational entropy gain arises from coupling a low-frequency protein vibration to ligand external motion.

2.2. All-Atom Model Systems and Calculations. The structural coordinates of DHFR with and without the ligand MTX were taken from the Protein Data Bank[48] entries, 1RX3 and 1RX1,[46] respectively. Energy minimizations and normal-mode analyses were performed using the program CHARMM, version 30b2.[49] The CHARMM all-atom parameter set 22[50] was used for the potential function. All pairwise electrostatic interactions were included, i.e., without truncation, and the dielectric constant was taken as distance-dependent ($\epsilon = r$) to roughly mimic solvation effects. Energy minimizations were performed using Adopted Basis Newton−Raphson (ABNR) minimization[49] until an rms energy gradient was reached of $<10^{-5}$ kcal/mol/Å. The mass-weighted second-derivative matrices calculated using the minimized structures were diagonalized to yield the normal-mode eigenvectors and eigenvalues.

2.3. Search for the Intermediate State. To examine to what extent the simplified models above might apply to realistic DHFR (+MTX) vibrational dynamics, an atomistic normal-mode analysis was performed using coordinates of the bound and unbound structures. To focus on the dynamical change by the ligand force field, the intermediate state, i.e., that with a structure similar to the bound state but without MTX bound, was derived using "iterative normal-mode analysis" as follows.

First, the crystal structure of the bound state was energy-minimized, leading to a structure we label "MinB". Second, a hypothetical system was constructed using the MinB coordinates but in which the interaction potential energy between the protein and the MTX was multiplied by $\alpha = 0.9$, and this system was again energy-minimized, yielding a new structure, "MinB09". This procedure was repeated sequentially decreasing α so as to derive the energy-minimum structures at $\alpha = 0.8$, 0.7, 0.6, 0.5, 0.4, 0.3, 0.2, 0.1, 0.05, and 0.01. Starting from MinB001, the MTX molecule was deleted, and the structure was again energy-minimized to obtain the intermediate state structure. Using the same iterative procedure in the reverse direction, the minimized structures at $\alpha = 1.1$, 1.2, 1.3, 1.4, and 1.5 were also derived.

At each minimized structure, a normal-mode analysis was performed to derive the frequency, ω_i, and eigenvector, $\mathbf{v}_i$, of each normal mode i. The $3N$-element ($N = N_P + N_L$) eigenvector of the complex was decomposed into the protein and MTX components, and further decomposition was performed of the MTX component into internal and external motions, i.e., $\mathbf{v}_i = \mathbf{v}_{i,\text{pro}} + \mathbf{v}_{i,\text{MTXint}} + \mathbf{v}_{i,\text{MTXext}}$. The ratio of each component was calculated as $R_{i,\text{pro}} = |\mathbf{v}_{i,\text{pro}}|^2/|\mathbf{v}_i|^2$, $R_{i,\text{MTXint}} = |\mathbf{v}_{i,\text{MTXint}}|^2/|\mathbf{v}_i|^2$, and $R_{i,\text{MTXext}} = |\mathbf{v}_{i,\text{MTXext}}|^2/|\mathbf{v}_i|^2$. The MTX internal and external motions were defined by the normal modes of the isolated MTX molecule. Using R_i, the vibrational entropy (eq 5) of the complex was also decomposed into each component: $S_{\text{vib,pro}}(\omega_i) = R_{i,\text{pro}}S_{\text{vib}}(\omega_i)$, $S_{\text{vib,MTXint}}(\omega_i) = R_{i,\text{MTXint}}S_{\text{vib}}(\omega_i)$, and $S_{\text{vib,MTXext}}(\omega_i) = R_{i,\text{MTXext}}S_{\text{vib}}(\omega_i)$.

The coupling constants between the protein and ligand normal modes in the complex, resulting from the interaction of the two modes, were calculated as the off-diagonal elements of the Hessian (second-derivative) matrix in the normal-mode representation. Using the $3N$-dimensional atomic (Cartesian) Hessian matrix, $\mathbf{H} = (H_{ij} = \partial^2 E/\partial x_i \partial x_j)$, the $3N_P$-dimensional protein eigenvector matrix, $\mathbf{V}_P = (\mathbf{v}_{P,1}, \mathbf{v}_{P,2}, \mathbf{v}_{P,3}, \cdots)$, and the $3N_L$-dimensional ligand eigenvector matrix, $\mathbf{V}_L = (\mathbf{v}_{L,1}, \mathbf{v}_{L,2}, \mathbf{v}_{L,3}, \cdots)$, the Hessian in the normal-mode representation is given by

$$\tilde{\mathbf{H}} = \mathbf{V}^t\mathbf{H}\mathbf{V} \qquad (6)$$

where

$$\mathrm{V} = \begin{pmatrix} \mathbf{V}_P & \mathbf{0} \\ \mathbf{0} & \mathbf{V}_L \end{pmatrix}$$

2.4. Vibrational Density of States. The vibrational density of states, $g(\omega)$, was calculated using the normal-mode frequencies, $\{\omega_i\}$, as

$$g(\omega) = \sum_{i=1}^{3N-6} \exp\left\{-\frac{(\omega - \omega_i)^2}{\sigma_i^2}\right\} \qquad (7)$$

where σ_i is the variance of the Gaussian distribution of each vibrational mode and represents, for example, a spectrometer instrumental resolution. $\sigma_i = 3$ cm^{-1} was used for all modes in this study. The protein and MTX internal and external contributions, $g_X(\omega)$ (where X = pro, MTX_{int}, MTX_{ext}) were calculated using R_X derived above as follows:

$$g_X(\omega) = \sum_{i=1}^{3N-6} R_{X,i} \exp\left\{-\frac{(\omega - \omega_i)^2}{\sigma_i^2}\right\} \qquad (8)$$

3. Results and Discussion

3.1. Vibrational Dynamics of the Unbound and Bound States. We first compare the bound- and unbound-state dynamics of DHFR using atomistic normal modes. The all-atom normal modes of both states were calculated, and the vibrational density of states and the vibrational entropy of the complex were

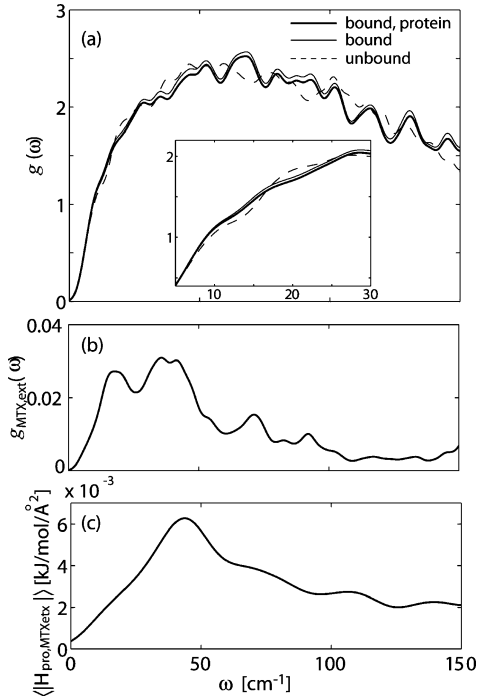

Figure 2. (a) Vibrational density of states, $g(\omega)$, from atomic-detail normal modes of the unbound (dashed curve) and bound (solid curve) states of DHFR. Protein contribution to the bound-state spectrum is also shown by the thick solid curve. Inset shows lowest-frequency spectra at $\omega < 30$ cm^{-1}. (b) $g(\omega)$ of MTX external motion derived from atomistic normal modes. (c) Coupling constants between protein vibrations and MTX external motions as a function of protein vibrational frequency in the intermediate state.

decomposed into contributions from the protein vibrations and the MTX internal and external motions.

The vibrational densities of states of the bound and unbound states, $g_{bound}(\omega)$ and $g_{unbound}(\omega)$, are shown in Figure 2a. In the low-frequency region $< \sim 20$ cm^{-1} $g_{bound}(\omega)$ has a slightly higher intensity than $g_{unbound}(\omega)$, in qualitative agreement with experiment.[32] The corresponding difference is also manifested in the vibrational entropy (eq 5) for $\omega < \sim 20$ cm^{-1} (i.e., summed over the 60 lowest-frequency normal modes): $T\Delta S_{vib} = TS_{vib,bound}$ ($\omega < \sim 20$ cm^{-1}) $- TS_{vib,unbound}$ ($\omega < \sim 20$ cm^{-1}) $= 223.4 - 222.2 = 1.2$ kJ/mol. The vibrational density of states of the intermediate state, $g_{intermediate}(\omega)$, is almost the same as $g_{bound}(\omega)$ (result not shown), indicating that conformational fluctuation around the bound state will not change $g_{bound}(\omega)$ significantly and will not affect the conclusion above.

The bound-state spectrum was decomposed into the protein ($g_{bound,pro}(\omega)$) and MTX internal and external contributions using eq 8. In Figure 2a, a small but clear difference is seen between $g_{bound}(\omega)$ and $g_{bound,pro}(\omega)$ in the low-frequency region <150 cm^{-1}, showing that, although $N_L \ll N_P$, the MTX contribution is considerable. Calculation of the vibrational entropy (eq 5) shows that the overall S_{vib} is larger in the bound state (7743 kJ/mol) than in the unbound state (7596 kJ/mol). However, the protein contribution, $S_{vib,pro}$, is smaller in the bound state (7536 kJ/mol): the protein vibrations themselves become stiffer on ligand binding. The increased S_{vib} on ligand binding, therefore, arises from the six degrees of freedom generated from MTX external motion ($TS_{vib,MTXext} = 36.1$ kJ/mol). The frequency distribution of the MTX external motion, $g_{MTXext}(\omega)$, calculated using the normal modes and eq 8, is shown in Figure 2b and indicates that the dominant contribution is in the lowest-frequency region <60 cm^{-1}.

The model derivation in eq 4 shows that the magnitude of the coupling constant quantifies the coupling strength. To examine the strength of the coupling between the protein and MTX external motions in the complex, the off-diagonal elements of the bound-state Hessian matrix, which relate the protein vibrations to the MTX external modes, were calculated using eq 6. The I and MinB001 states (see section. 2.3) were used as the unbound and bound states in this calculation because both structures are almost the same (the average mean-square deviation between the two structures is 0.033 Å^2). The absolute value of the coupling constant averaged over the six MTX external modes, shown in Figure 2c as a function of protein frequency in the unbound state, indicates that the MTX external motion couples more strongly to the protein low-frequency modes with $\omega < 100$ cm^{-1} than to those at higher frequency. The frequency of the maximum coupling constant, i.e., the peak position, is higher than that of $g_{MTXext}(\omega)$, in agreement with the analytical model derivation in which the frequency in the complex is lower than the protein frequency without ligand binding, i.e., $\omega^2 < \omega_p^2/2$ (see Figure 1c).

In conclusion, dynamical softening on ligand binding originates from the motion in the complex in which the protein vibrations are coupled to the MTX external motion, whereas the protein internal motion itself becomes stiffer.

3.2. Pathway Analysis of the Ligand-Binding Process from Intermediate to Bound State. Iterative energy minimizations were performed of the bound state in which the protein−ligand interaction was multiplied by a scaling factor, α. The intermediate state without ligand bound was obtained as the structure at $\alpha = 0$. α was used as the "reaction coordinate" determining the pathway from the intermediate to the bound state. The vibrational entropy of the protein and the MTX internal and external motions were calculated as a function of α.

In Figure 3a the mean-square deviation averaged over the protein atoms, Δx^2, is plotted as a function of α. Δx^2 from the bound (B) state increases slightly with $|\alpha - 1|$ from that at $\alpha = 1$, indicating that a gradual decrease or increase in the ligand interaction strength from the bound state ($\alpha = 1$) through the iterative energy minimization processes avoids drastic structural change of the protein. Relative to the unbound state (U), all the α states have $\Delta x^2 = 1.4-1.6$ Å^2: this is much larger than Δx^2 between the I and B states (0.55 Å^2), validating the assumption that the conformational change occurs mainly in process 1 (U → I, see Figure 1a). The increase of Δx^2 from the U state and the decrease of Δx^2 from the B state during the process from $\alpha = 0$ to 1 is consistent with the I state being on the pathway of the ligand-binding process; i.e., the I state is a structure intermediate between those of U and B.

In Figure 3b the interaction energy between the DHFR and MTX, E_{int}, is shown as a function of α. The straight line, fitted through the data points at $\alpha = 0$ (I) and $\alpha = 1$ (B), corresponds to E_{int} calculated in the absence of structural change from the bound state, $E_{int}(\alpha)$, i.e., while keeping all the coordinates fixed at the B state. The deviations from this line are small at all α, again consistent with the structural change occurring mainly in process 1 (from U to I). However, the deviation is systematic, corresponding to a shallow convex curve of $E_{int}(\alpha)$. This convexity indicates that the slight structural change that does occur results in stabilization of the complex energetically, i.e., enthalpically, with increasing binding strength. The gain of interaction energy via structural change from the I state, Δ, was evaluated as follows: first, $E_{int}(\alpha)$ was fitted to a quadratic function of α (the resulting function is $E_{int} = -110\alpha^2 - 510\alpha$

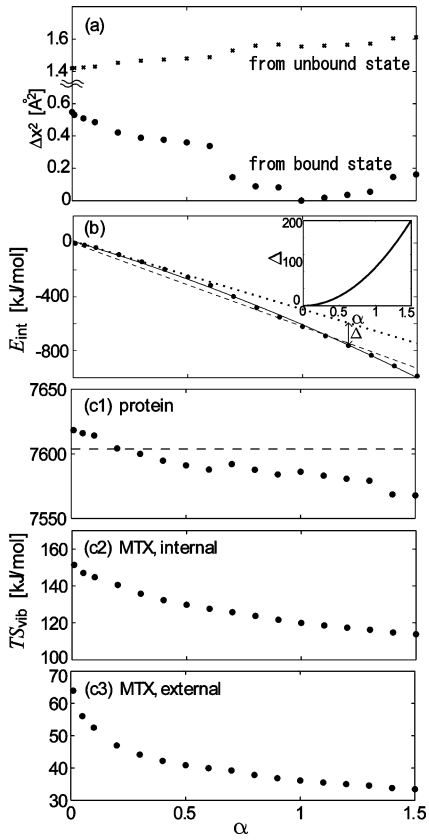

Figure 3. Dependence on the protein:ligand binding strength scaling factor, α, of (a) mean-square deviations, Δx^2, from the bound (dot) and unbound (cross) structures, (b) interaction energy between DHFR and MTX, E_{int}, and (c) vibrational entropies, TS_{vib}, associated with (c1) the protein vibrations, (c2) the MTX internal motion, and (c3) the MTX external motion. In (b), the fitted curve of $E_{int}(\alpha)$ is also shown as well as a straight line fitted through the data points at $\alpha = 0$ (I) and 1 (U) (dashed line) and the tangent line at $\alpha = 0$ (dotted line). The interaction energy gain via structural change from the I state, Δ, is also shown in the inset. See text for details.

+13 [kJ/mol]) and then the tangent line at $\alpha = 0$ of the fitting curve derived. This tangent is E_{int} in the absence of structural change from the I state. Δ, calculated as the difference between $E_{int}(\alpha)$ and the tangent line, increases quadratically with α, indicating that the complex formation is stabilized by binding strength via structural change.

In Figure 3c the vibrational entropy of the protein and the MTX internal and external motion are shown as a function of α. These three quantities decrease with α, indicating shifts of these motions to high frequency. This result shows that the prediction by the model derivation in eq 2 and eq 4 is applicable to the all-atom representation of protein−ligand binding.

The limits of $S_{vib,pro}$ and $S_{vib,MTXint}$ at $\alpha = 0$ provide S_{vib} in the intermediate state (~7619 kJ/mol) and the entropy of free MTX (~151 kJ/mol). S_{vib} in the I state is larger than that in the U state by ~23 kJ/mol. This may be another reason for the dynamical softening via ligand binding: i.e., the structure undergoes a conformational change from the U to I state such that the system gains vibrational entropy. The free energy associated with the entropy change during the binding process is $T\Delta S = TS_{vib,bound} - TS_{vib,unbound} - TS_{vib,MTX} = \sim -4$ kJ/mol.

In summary, the dynamical softening via MTX binding to DHFR arises from (1) the weak protein:ligand interaction preventing much loss of the complex entropy and (2) the larger entropy of the intermediate state relative to the unbound state. The decrease of the vibrational entropy with α implies that, for complexes stabilized with larger α (i.e., stronger interaction energy), increased entropy on ligand binding (i.e., dynamical softening) would not be observed. Consequently, the binding strength in the complex is determined by the balance between the enthalpic and entropic contributions so as to minimize the free energy.

4. Conclusions

In the work presented here the change of internal protein dynamics on ligand binding has been examined using a simple analytical "ball-and-string" model and all-atom normal-mode analysis. The analytical model system comprises two degrees of freedom coupled with a harmonic spring and is used to understand the physics behind dynamical changes in the complex on ligand binding, providing insight useful for interpreting the results of atomistic normal-mode analyses of a model protein, DHFR, with and without the therapeutic ligand MTX bound.

In the analytical model, an entropy-rich, low-frequency vibration is generated by the coupling between the protein vibration and the ligand external motion, although shifts to higher frequency occur from the coupling of protein and ligand vibrations. The lower-frequency motion generated is likely to be a contribution to experimentally observed softening of complex vibrations upon ligand binding.[32]

Atomistic normal-mode analysis of MTX-bound and unbound DHFR was performed, and the results were compared with the analytical models. A slight but statistically significant difference in the vibrational densities of states between the bound and unbound states is seen at $\omega < \sim 20$ cm^{-1}, in accord with previous findings from normal-mode calculations on water binding to BPTI[28,29] and insulin dimerization,[25] and a corresponding change is found in the vibrational entropy, which is qualitatively similar but quantitatively smaller than that observed in neutron-scattering experiments.[32]

The atomistic NMA of the bound and unbound states revealed a large contribution of the MTX external motion to the increased entropy (~36 kJ/mol). This is remarkably large given that only six degrees of freedom are involved. The MTX external contribution to the vibrations of the complex is found mostly in the low-frequency region (<60 cm^{-1}), in agreement with the simplified model derivation, involving coupling of MTX external motion with low-frequency protein vibrations (<100 cm^{-1}). The frequency at which the coupling constant is maximum is higher than that of $g_{MTXext}(\omega)$, again in accord with the model derivation in which the complex frequency generated is lower than the unbound protein frequency; i.e., $\omega^2 < \omega_p^2/2$.

Iterative energy minimizations of the bound state, B, while decreasing step-by-step the protein−ligand interaction energy, were performed to derive a hypothetical "intermediate" state, I, i.e., with a structure similar to the bound state but without the ligand, MTX. The process of going from I to B was studied as a function of the protein−ligand interaction energy scaling factor, α. The entropies of the protein and the MTX internal and external contributions were found to decrease with α, indicating that a shift to high frequencies of the vibration in the complex originates from the ligand force field. This result is also in agreement with the analytical model. Simultaneously, the complex gains interaction energy so as to stabilize the structure.

The entropies of the protein and MTX internal motions at the limit $\alpha = 0$ provide the entropy of the intermediate state, $S_{vib,I}$, and of free MTX, $S_{vib,MTX}$. The increased entropy of I

relative to U is a further contribution to softening of the vibrations of the complex on ligand binding; i.e., the protein undergoes a conformational change from U to I resulting in a vibrational entropy gain. The vibrational entropy change on binding, ΔS, is ~ -4 kJ/mol. Although in qualitative agreement in the low-frequency vibrational spectrum, ΔS is lower than the experimental value of $\sim 25 \pm 6$ kJ/mol.[32] The difference may originate from anharmonicity and/or environmental effects, neither of which were estimated in the present atomistic harmonic analysis.

During the ligand-binding process, as followed through the iterative energy minimizations, the vibrational entropy of the complex decreases with increasing binding strength. The thermodynamics at the final bound state will be determined by the free energy compensation between the enthalpy (i.e., the configurationally averaged interaction energy) and the vibrational entropy. In case of the DHFR and MTX complex, the ligand interaction will be enthalpically weak enough that the loss of the vibrational entropy in the complex via ligand force generation is smaller than the entropy gain through the coupling between the protein and MTX external motions, thus resulting in dynamical softening upon ligand binding.

The following two assumptions were made in the present study: (1) that the ligand-binding process can be decomposed theoretically into the protein conformational change followed by the generation of the ligand force field and (2) the validity of the harmonic approximation. The former assumes the "population shift" model[51] for ligand binding, in which the native state of the protein exhibits an ensemble of conformations covering both the bound and unbound structures and the ligand will bind selectively to the bound-state structure, thereby biasing the equilibrium toward the binding conformation. This contrasts with the "induced-fit" model,[52] in which the intermediate state has the same structure as the unbound state and the conformational change is driven by the generation of the ligand force. In the present study, the U to I conformational change is much larger than that of I to B, tending, then, toward the population shift model. However, the real ligand-binding process will be situated between the above two extreme models. The small structural change that does occur between I and B via induced fit may stabilize the complex structure via a decrease in the interaction energy with α. Concerning the use of the harmonic approximation, anharmonic contributions are essential to a complete quantitative study of ligand-binding thermodynamics at physiological temperatures. However, the two above assumptions in combination with simplified analytical models and atomistic NMA are appropriate for obtaining a simplified picture of the physical origin of the vibrational component of ligand-binding thermodynamics.

The detailed analysis of the conformational change from the unbound to intermediate state will be a future project. Understanding whether and when protein−ligand complexes are formed due to entropy- or enthalpy-driven binding, and which complexes are closer to the induced fit or population shift models, will form a basis for understanding the process of ligand binding to protein molecules. More generally, the present work illustrates how the interpretation of judiciously decomposed complex atomistic simulations with simple analytical models can provide fundamental insight into the physics underlying basic biochemical processes.

Acknowledgment. We thank Dr. E. Balog for helpful comments and Dr. M. Krishnan for useful discussions. J.C.S. acknowledges funds from the U.S. Department of Energy via a Laboratory-Directed Research and Development grant. K.M. acknowledges support by the MEXT grand challenge program using next-generation supercomputing.

References and Notes

(1) Klotz, I. M. *Q. Rev. Biophys.* **1985**, *18*, 227.
(2) Benkovic, S. J.; Fierke, C. A.; Naylor, A. M. *Science* **1988**, *239*, 1105.
(3) Lian, L. Y.; Barsukov, I. L.; Sutcliffe, M. J.; Sze, K. H.; Roberts, G. C. *Methods Enzymol.* **1994**, *239*, 657.
(4) Lamb, M. L.; Jorgensen, W. L. *Curr. Opin. Chem. Biol.* **1997**, *1*, 449.
(5) Wang, W.; Donini, O.; Reyes, C. M.; Kollman, P. A. *Annu. Rev. Biophys. Biomol. Struct.* **2001**, *30*, 211.
(6) Frauenfelder, H.; Sligar, S. G.; Wolynes, P. G. *Science* **1991**, *254*, 1598.
(7) Frauenfelder, H.; Parak, F.; Young, R. D. *Annu. Rev. Biophys. Biophys. Chem.* **1988**, *17*, 451.
(8) Karplus, M.; McCammon, J. A. *Nat. Struct. Biol.* **2002**, *9*, 646.
(9) Carl, N.; Konc, J.; Janežič, D. *J. Chem. Inf. Mod.* **2008**, *48*–1279.
(10) Tama, F.; Brooks, C. L., III. *J. Mol. Biol.* **2002**, *318*, 733.
(11) Tama, F.; Wriggers, W.; Brooks, C. L., III. *J. Mol. Biol.* **2002**, *321*, 297.
(12) Tama, F. *Protein Pept. Lett.* **2003**, *10*, 119.
(13) Tama, F.; Miyashia, O.; Brooks III, C. L. *J. Mol. Biol.* **2004**, *337*, 985.
(14) Ma, J. *Curr. Protein Pept. Sci.* **2004**, *5*, 119.
(15) Ikeguchi, M.; Ueno, J.; Sato, M.; Kidera, A. *Phys. Rev. Lett.* **2005**, *94*, 078102.
(16) Miyashita, O.; Onuchi, J. N.; Wolynes, P. G. *Proc. Natl. Acad. Sci. U.S.A.* **2003**, *100*, 12570.
(17) Nadig, G.; Vishveshwara, S. *Biopolymers* **1997**, *42*, 505.
(18) Radkiewicz, J. L.; Brooks, C. L. *J. Am. Chem. Soc.* **2000**, *122*, 225.
(19) Vitagliano, L.; Merlino, A.; Zagari, A.; Mazzarella, L. *Proteins* **2002**, *46*, 97.
(20) Merlino, A.; Vitagliano, L.; Ceruso, M. A.; Nola, A. D.; Mazzarella, L. *Biopolymers* **2002**, *65*, 274.
(21) Lai, Y.-T.; Cheng, C.-S.; Liu, Y.-N.; Liu, Y.-J.; Lyu, P.-C. *Proteins* **2008**, *72*, 1189.
(22) Brooks, B. R.; Karplus, M. *Proc. Natl. Acad. Sci. USA* **1985**, *82*, 4995.
(23) Gibrat, J. F.; Go, N. *Proteins: Struct., Funct., Genet.* **1990**, *8*, 258.
(24) Seno, Y.; Go, N. *J. Mol. Biol.* **1990**, *216*, 95.
(25) Tidor, B.; Karplus, M. *J. Mol. Biol.* **1994**, *238*, 405.
(26) Perahia, D.; Mouawad, L. *Comput. Chem.* **1995**, *19*, 241.
(27) Mouawad, L.; Perahia, D. *J. Mol. Biol.* **1996**, *258*, 393.
(28) Fischer, S.; Verma, C. S. *Proc. Natl. Acad. Sci. U.S.A.* **1999**, *96*, 9613.
(29) Fischer, S.; Smith, J. C.; Verma, C. S. *J. Phys. Chem. B* **2001**, *105*, 8050.
(30) Tama, F.; Sanejouand, Y. H. *Protein Eng.* **2001**, *14*, 1.
(31) Delarue, M.; Sanejouand, Y. H. *J. Mol. Biol.* **2002**, *320*, 1011.
(32) Balog, E.; Becker, T.; Oettl, M.; Lechner, R.; Daniel, R.; Finney, J.; Smith, J. C. *Phys. Rev. Lett.* **2004**, *93*, 028103.
(33) Stone, M. J. *Acc. Chem. Res.* **2001**, *34*, 379.
(34) Schnell, J. R.; Dyson, H. J.; Wright, P. E. *Annu. Rev. Biophys. Biomol. Struct.* **2004**, *33*, 119.
(35) Yamniuk, A. P.; Nguyen, L. T.; Hoang, T. T.; Vogel, H. J. *Biochemistry* **2004**, *43*, 2558.
(36) Ainavarapu, S.; Li, L.; Badilla, C. L.; Fernandez, J. M. *Biophys. J.* **2005**, *89*, 3337.
(37) Fierke, C. A.; Johnson, K. A.; Benkovic, S. J. *Biochemistry* **1987**, *26*, 4085.
(38) Andrew, J.; Fierke, C. A.; Birdsall, B.; Ostler, G.; Feeney, J.; Roberts, G. C. K.; Benkovic, S. J. *Biochemistry* **1989**, *28*, 5743.
(39) Fleischman, S. H.; Brooks, C. L., III. *Proteins* **1990**, *7*, 52.
(40) Radkiewicz, J. L.; Brooks, C. L., III. *J. Am. Chem. Soc.* **2000**, *122*, 225.
(41) Rod, T. H.; Radkiewicz, J. L.; Brooks, C. L., III. *Proc. Natl. Acad. Sci. U.S.A.* **2003**, *100*, 6980.
(42) Huennekens, F. M. *Enzyme Regul.* **1994**, *34*, 397 Adv.
(43) Brooks, B. R.; Janei, D.; Karplus, M. *J. Comput. Chem.* **1995**, *16*, 1522.
(44) Janežič, D.; Praprotnik, M.; Merzel, F. *J. Chem. Phys.* **2005**, *122*, 174101.
(45) Goupil-Lamy, A. V.; Smith, J. C.; Yunoki, J.; Parker, S. F.; Kataoka, M. *J. Am. Chem. Soc.* **1997**, *119*, 9268.
(46) Sawaya, M. R.; Kraut, J. *Biochemistry* **1997**, *36*, 586.

(47) McQuarrie, D. A. *Statistical Mechanics*; Harper Row: New York, 1976.

(48) Berman, H. M.; Westbrook, J.; Feng, Z.; Gilliland, G.; Bhat, T. N.; Wessig, H. *Nucleic Acids Res.* **2000**, *28*, 235.

(49) Brooks, B. R.; Bruccoleri, R. E.; Olafson, B. D.; States, D. J.; Swaminathan, S.; Karplus, M. *J. Comp. Biol.* **1983**, *4*, 187.

(50) MacKerell, A. D., Jr.; Bashford, D.; Bellott, R. L.; Dunbrack, R. L., Jr.; Evanseck, J. D.; Field, M. J.; Fischer, S.; Gao, J.; Guo, H.; Ha, S.; Joseph-McCarthy, D.; Kuchnir, L.; Kuczera, K.; Lau, F. T. K.; Mattos, C.; Michnick, S.; Ngo, T.; Nguyen, D. T.; Prodhom, B.; Reiher, W. E., III; Roux, B.; Schlenkrich, M.; Smith, J. C.; Stote, R.; Straub, J.; Watanabe, M.; Wiorkiewicz-Kuczera, J.; Yin, D.; Karplus, M. *J. Phys. Chem. B* **1998**, *102*, 3586.

(51) Tsai, C. J.; Kumar, S.; Ma, B.; Nussinov, R. *Protein Sci.* **1999**, *8*, 1181.

(52) Koshland, D. *Proc. Natl. Acad. Sci. U.S.A.* **1958**, *44*, 98.

JP909677P